ELSEVIER

Ceramics International 27 (2001) 15–24

CERAMICS INTERNATIONAL

www.elsevier.com/locate/ceramint

Laser cladding of yttria partially stabilized ZrO_2 (YPSZ) ceramic coatings on aluminum alloys

J.H. Ouyang *, S. Nowotny, A. Richter, E. Beyer

Fraunhofer Institute for Material and Beam Technology, Winterbergstrasse 28, D-01277 Dresden, Germany

Received 8 March 2000; received in revised form 9 March 2000; accepted 24 March 2000

Abstract

A feasibility study of laser clad 7 wt.% yttria partially stabilized zirconia ceramic coatings undoped or doped with 2.5 wt.% TiO_2 to produce single tracks and partially overlapped tracks on the surfaces of AlSi9Cu3, AlZn10Si8Mg and AlSi10Mg alloys was carried out by using a 6 kW RS5000 continuous wave CO_2 laser together with continuous powder-feeding system. The dependencies of the macro and microquality of ZrO_2 ceramic coatings on the properties of the coating powder and laser parameters, and microstructure (such as morphology, phase transformation, etc.) were studied. The addition of 2.5 wt.% TiO_2 into the YPSZ powder is beneficial for the controllable cracking in the ceramic layer on AlSi9Cu3 alloy. The ceramic layers on three kinds of aluminum alloys exhibit planar ZrO_2 crystals with different sizes at the lower, columnar grains in the intermediate, and equiaxed grains at the upper region of the cross-sections. Small amounts of molten aluminum alloy are observed to segregate at the boundary regions of columnar or equiaxed grains in the ZrO_2 layer because of the poor affinity. The ceramic layers consist mainly of non-transformable t' phase and small amount of the retained c phase. Under conditions of optimum laser parameters and coating powder properties, the bonding to aluminum alloys is satisfactory with small dilution. Molten aluminum alloy is also observed to flow into the cracked ZrO_2 layer at the bottom to seal these cracks. The hardness of the ZrO_2 ceramic layer was 1415–1575 HV0.1, which is mainly attributed to the absence of porosity and fine grains in the ceramic layers.

Keywords: B. Grain boundaries; C. Toughness and toughening; D. TiO_2; D. ZrO_2; D. Y_2O_3; Laser cladding

1. Introduction

Because of their high strength-to-weight ratios, aluminum alloys have found widespread use in transportation engineering applications. However, the relatively low thermal barrier performance of aluminum alloys is one of the major factors that restrict their potential application in automotive hot section components. Usually, plasma spraying of yttria partially stabilized zirconia powders has been most widely developed as a process to improve the efficiency and performance of turbine and diesel engine hot section components in high temperature applications. However, the commonly existing porosity in the deposits and the weak adhesion to the substrate formed by plasma spraying affect the performance of TBCs and often lead to premature degradation and failure because of condensed salt and oxygen penetration at high temperatures and spallation of TBCs [1].

An approach to solve this problem is to clad yttria partially stabilized ZrO_2 ceramic coatings by one-step laser cladding. Investigations [2,3] have been performed to produce thick and dense ZrO_2 ceramic coatings with controlled cracks and relatively fine substructure. But these coatings were mainly clad on superalloy or steel. Only a very few work was found to laser-clad ceramic coatings on aluminum alloys [4,5]. In addition, the major problem associated with this technique is the cracking and spalling of the ceramic coatings due to thermal stress during rapid solidification. In fact, cracking of oxide ceramic coatings during laser cladding is very hard to avoid. Cracks in the ceramic layer parallel to the surface are very detrimental to TBC lifetime because of spallation, but vertical cracks are generally considered to be beneficial to accommodate the strain occurring during thermal cycling [6].

* Corresponding author at present address: Tribology Division, Mechanical Engineering Laboratory (MEL), AIST/MITI, 1-2 Namiki, Tsukuba, Ibaraki 305-8564, Japan. Tel.: +81-298-617196; fax: +81-298-617007.

E-mail address: ouyangjh@hotmail.com (J.H. Ouyang).

0272-8842/01/$20.00
PII: S0272-8842(00)00036-5

Some proposals [2,6–8] were given to control the number and type of cracks in ceramic coatings. Controllable cracking is very beneficial for fatigue properties since it allows accommodation of thermal stress produced during service under thermal cycling. Segmented cracks produced by laser glazing [8] were found to improve the strain accommodation and finally lead to a fourfold thermal cyclic lifetime extension of TBCs, in comparison with plasma-sprayed TBCs. Nowotny and coworkers [4,5] used the one-step laser cladding technique to clad dense, non-porous Al_2O_3/TiO_2-layers with a good bonding strength and only a few vertical cracks on aluminum alloys. The results of Ruckle [9], Grot and Martyn [10] indicated that the segmented cracks significantly improve the lifetime of plasma-sprayed TBCs, whereas dense crack-free coatings showed poor performance.

In the present work, a feasibility study has been made by using one-step laser cladding to produce YPSZ ceramic coatings, which are thick, dense and only contain a few controllable cracks, on several aluminum alloys. The microstructure and hardness of the ZrO_2 coating are analyzed, and the effects of laser processing parameters and coating powder characteristics on the macro and microquality of ZrO_2 ceramic coatings are also discussed.

2. Experimental procedure

The substrate materials used in this investigation were three kinds of aluminum alloys: AlSi9Cu3, AlZn10-Si8Mg and AlSi10Mg. Seven wt.% yttria partially stabilized zirconia (YPSZ) powder with an average particle size of 67.5 μm was used as coating material. In order to reduce the thermal stress mismatch and solidification shrinkage defects, a mixture of 97.5 wt.% YPSZ and 2.5 wt.% TiO_2 powders with a particle size range from 45 to 90 μm was also injected into the melt pool of some AlSi9Cu3 samples. Laser cladding was carried out by using a Rofin-Sinar RS5000 6 kW continuous wave CO_2 laser. Before cladding, specimen surface was carefully cleaned with alcohol. The laser was operated in a (transverse electromagnetic) TEM_{20} mode with a defocused beam of about 3 mm diameter. Argon gas was used as the feeding gas. The laser cladding parameters were selected as 1.1–2.0 kW laser power, 3 mm beam diameter and 150–700 mm/min traverse speed. Partially overlapped tracks with 30 and 50% overlap coefficients were produced by controlling the computer program. The cladding powder was delivered to the melt pool via a double-hopper powder feeder. The powder feed rate was in the range from 4 to 12 g/min.

Laser-clad specimens were carefully sectioned using an abrasive diamond wheel. Before sectioning a cold mounting with an epoxy adhesive was applied to ensure that the coating did not peel off during sectioning. The cross-sectioned samples were ground and polished successively by using a special coating preparation procedure. Measurements of laser track width and thickness were carried out by using an optical microscope. Microhardness measurements with a 100 g test load have been made on the cross-sections after grinding and polishing by using a Struers HMV-2000 microhardness tester. Microstructural characterization of laser-clad ceramic layers was observed by using a high resolution optical microscope, and a Jeol JSM6400 scanning electron microscope equipped with an energy dispersive X-ray spectrometer and operated at 15 kV voltage. The phases in the initial powder and laser clad ceramic layers were identified by using a Siemens D5000 X-ray diffractometer with 40 kV operating voltage and CoK_α radiation. A labeling program was used in the range $20^\circ < 2\theta < 100^\circ$ at a 2θ scanning speed of 2° min^{-1}. A step scanning program using a 2θ scanning rate of 0.02° s^{-1} was employed to determine the intensity of the peaks for values of 2θ in the range 32–38° and 86–91°. These intensities were used to evaluate the proportions of the m, c, t, t' phases.

3. Results and discussion

3.1. General features of the ceramic layers

Single tracks and partially overlapped tracks with a thickness in the range from 0.5 to 1.0 mm were produced on different aluminum alloys under a wide range of laser parameters and feeding rates. Fig. 1 shows optical micrographs of the general morphologies of laser clad ZrO_2 ceramic coatings without TiO_2 addition on different aluminum alloys. Relatively dense ZrO_2 structure together with a lot of various cracks is observed from these cross-section micrographs. The profile of the tracks has been found to depend mainly on the powder feed rate, specific energy and overlap coefficient. The traverse speed and powder feed rate have a distinct influence on the build-up of the clad layers, while laser power mainly affects the melt thickness of aluminum alloys. At high feeding rates and slow traverse speeds, thick ceramic layers for single track were obtained. The thickness of coating at the overlapped region depends mainly on the overlap coefficient used.

A large number of shrinkage cavities in the penetration zone of AlSi9Cu3 alloy are caused by excessive energy input as shown in Fig. 2, although only few vertical cracks are observed in the partially overlapped ceramic layer by using the mixed powder with TiO_2 addition. The extent of substrate melting is affected either by the increase of power or by the decrease of traverse speed. But under this experimental condition laser power exhibits greater effect on the melting of the substrate than traverse speed. For AlZn10Si8Mg alloy, high laser power density and low traverse speed is needed to clad ZrO_2 ceramic coatings with the same thickness in contrast to

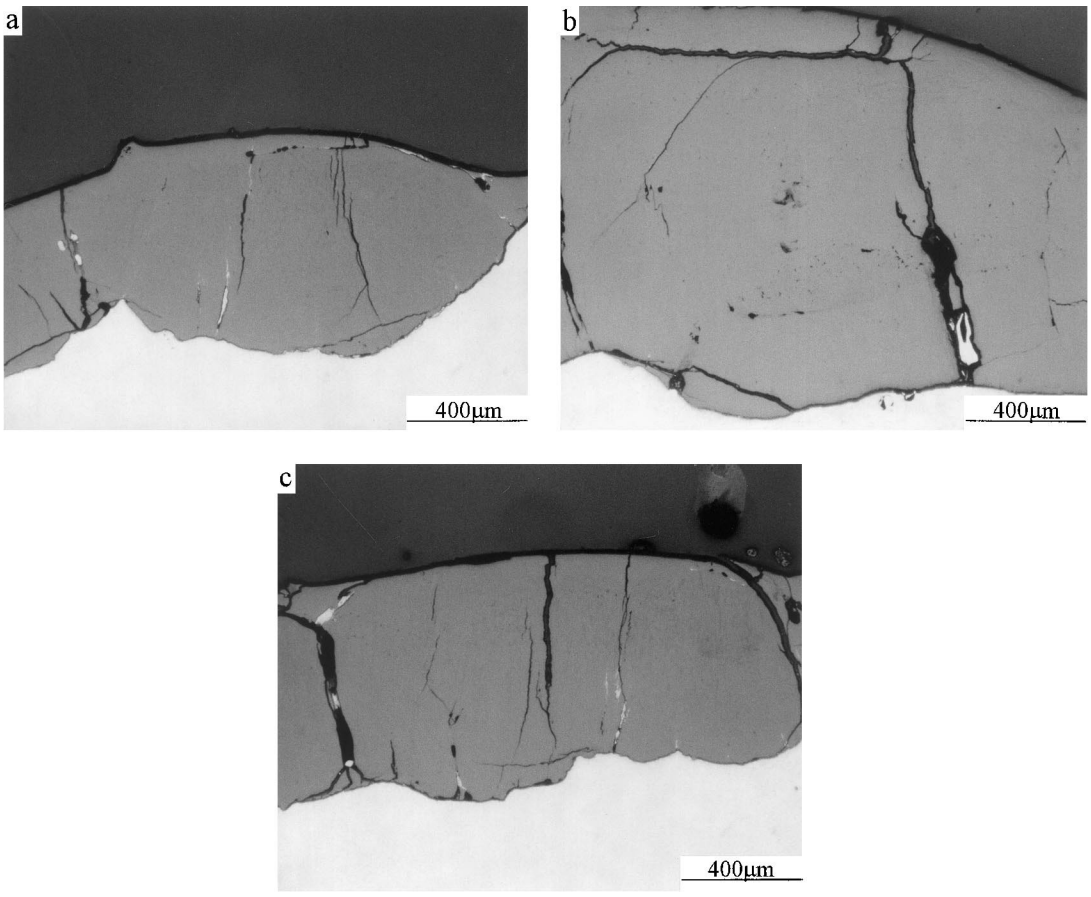

Fig. 1. Optical micrographs showing the morphologies of ZrO_2 ceramic layers without TiO_2 addition on different aluminum alloys: (a) on AlSi10Mg alloy; (b) on AlSi9Cu3 alloy; (c) on AlZn10Si8Mg alloy.

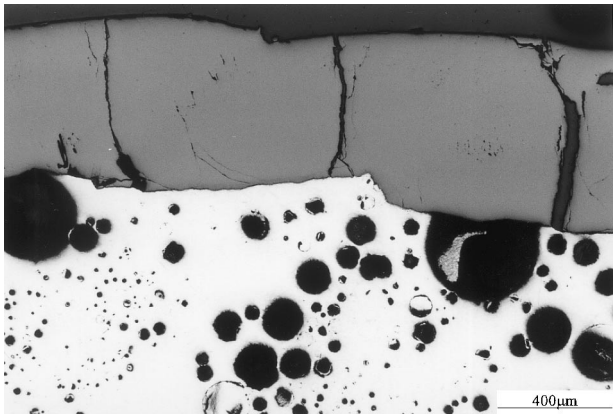

Fig. 2. Optical micrographs showing the shrinkage cavity in the penetration zone of AlSi9Cu3 alloy clad with a mixed powder of YPSZ and 2.5 wt.% TiO_2.

AlSi10Mg and AlSi9Cu3 alloys. In this investigation, an increase of 200 W in laser power must be used to produce the coatings on AlZn10Si8Mg alloy. This is attributed to the effect of substrate thermal properties on the cladding process of ceramic coating. Penetration of zirconia into the aluminum alloys to produce a concave profile is very different in comparison to those obtained with NiCoCrAlY bond coat on steel or superalloy. No typical convex dimension but relatively planar surface is obtained (Figs. 1 and 2). Substantial melting of aluminum alloys easily causes formation of shrinkage cavities in the Al-penetration zone and a largely irregular bonding interface between the ZrO_2 coatings and the Al-penetration zone.

3.2. Cracking and bonding

Many observations of the clad ZrO_2 surfaces on aluminum alloys demonstrate that the top views of ceramic coatings were characterized by a fine network of cracks. The cross-sections in Figs. 1 and 3 show the morphologies of different cracks in the ceramic layers on aluminum alloys. At lower traverse speed and high feeding rate, the increase in coating thickness strongly leads to horizontal cracking and spallation of the coatings (Figs. 1b and 3a). In addition to the coarse and primary vertical cracks, the clad layers exhibit fine secondary vertical cracks and horizontal cracks as shown in Fig. 3b, which probably lead to partial spallation of the coating. Cracking is undoubtedly due to thermal stresses developed during

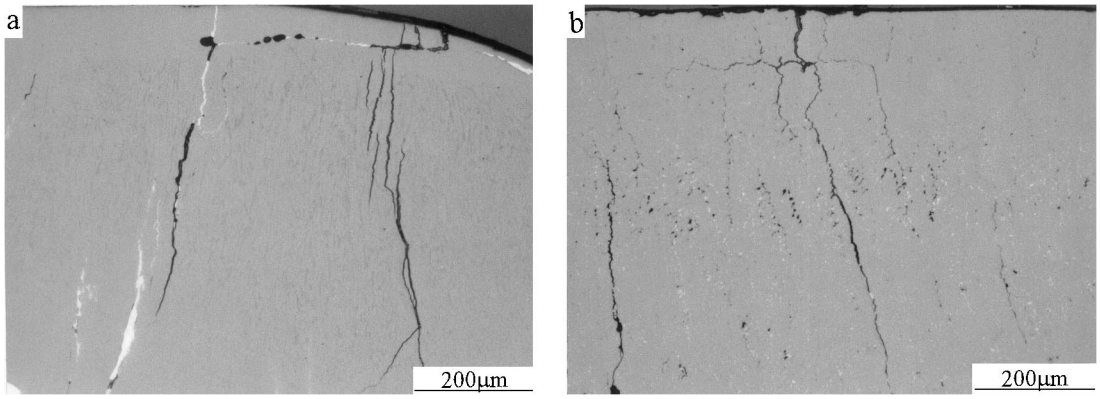

Fig. 3. Cross-sections showing the morphologies of vertical and horizontal cracks in laser-clad ZrO_2 ceramic layers without TiO_2 addition on different aluminum alloys: (a) on AlSi10Mg alloy; (b) on AlZn10Si8Mg alloy.

rapid solidification, although some cracks might have occurred during sectioning or polishing. It seems very difficult to avoid the cracking only by changing the laser parameters and the coating powder variables. In order to control the horizontal cracking which leads to spallation, an approach is done to reduce the excessive thermal stress concentration in the ZrO_2 layers induced by the laser melting and rapid cooling process. In the present work 2.5 wt.% TiO_2 was added to the YPSZ powder to reduce the thermal stress and solidification shrinkage of the ceramic coatings on AlSi9Cu3 alloy. Fig. 4 shows the controlled microcracking obtained by injecting the mixed powder of YPSZ doped with 2.5 wt.% TiO_2 on AlSi9Cu3 alloy. At low laser power, slow traverse speed and intermediate feeding rates, it is possible to obtain controllable cracking and make the treated surface relatively smooth, dense, very hard (see the indents in Fig. 4) mainly with reduced vertical cracks (also see Figs. 2, 5, 6 and 11). The perpendicular or through-thickness cracks do not contribute to spallation of coating and also may have the beneficial effect of arresting cracks during the thermal fatigue process before they cause substantial damage to the overall coating integrity.

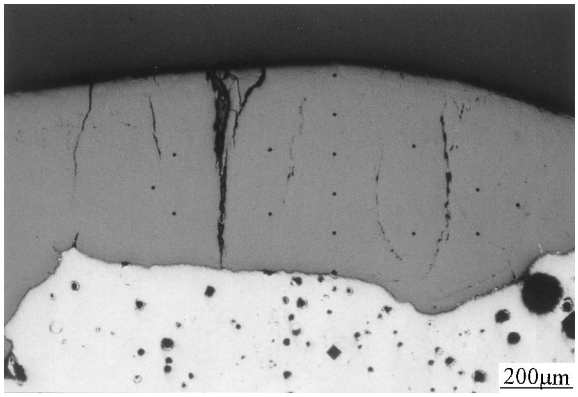

Fig. 4. Controlled microcracking obtained by injecting the mixture of YPSZ and 2.5 wt.% TiO_2 powder on AlSi9Cu3 alloy.

The partially overlapped tracks with layers about 0.5–1.0 mm thick on AlSi9Cu3 alloy obtained by using the mixed powder doped with 2.5 wt.% TiO_2 show a relatively smooth surface and controllable cracking. Fig. 5 shows the vertical cracks at the overlapped zone with different overlap coefficients by injecting the mixed powder doped with TiO_2. These claddings on AlSi9Cu3 alloy

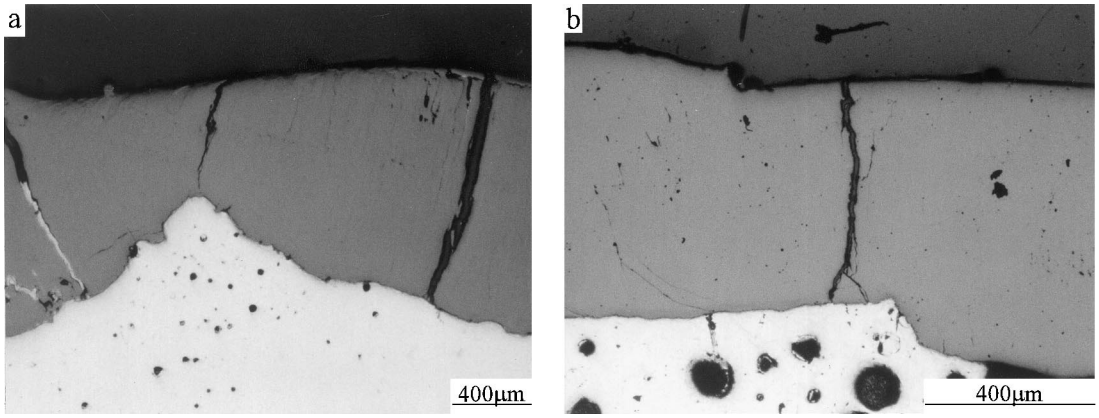

Fig. 5. Optical micrographs showing the vertical cracks at the overlapped zone with different overlap coefficient by injecting the mixture of YPSZ and 2.5 wt% TiO_2 on AlSi9Cu3 alloy: (a) overlap coefficient 30%; (b) overlap coefficient 50%.

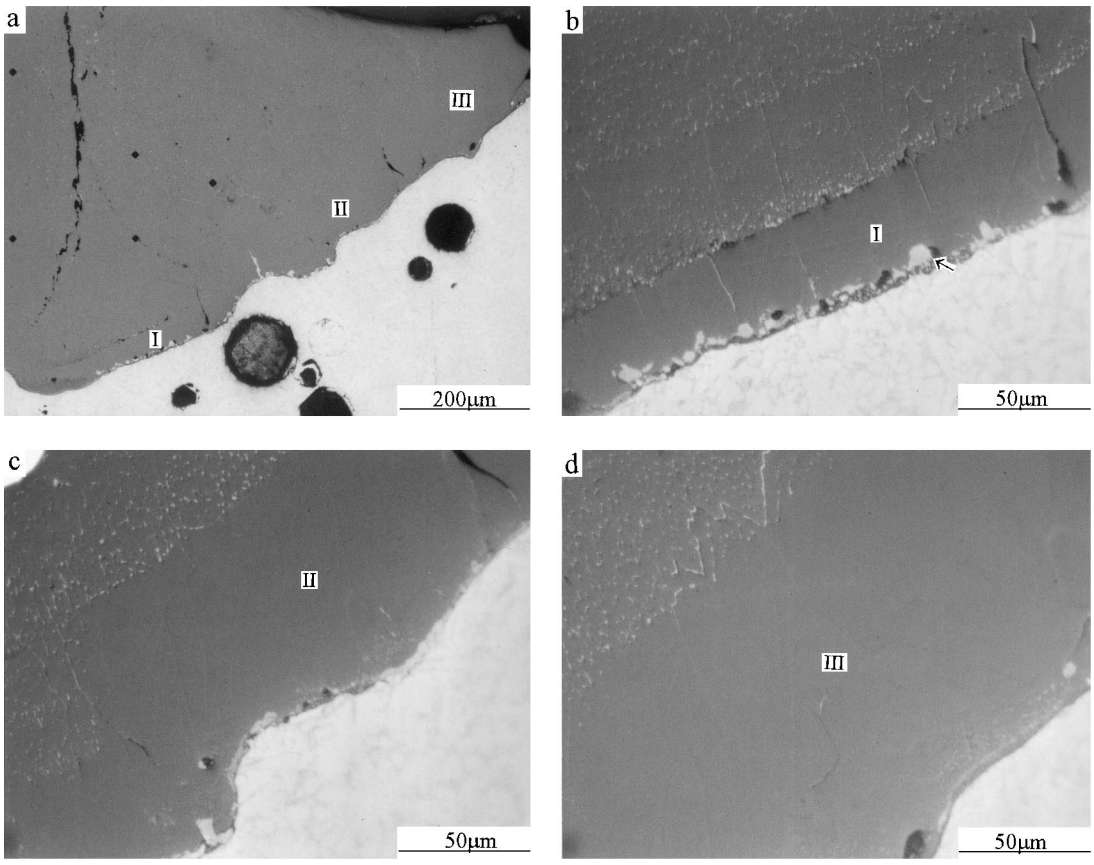

Fig. 6. Interfacial bonding showing different thickness of planar ZrO_2 crystal from the center to the edge of the laser track on AlSi9Cu3 alloy by using the mixed powder with TiO_2 addition: (a) low magnification interfacial characteristics; (b)–(d) planar ZrO_2 crystals with different thickness from the center to the edge.

can be achieved with minimum shrinkage cavities under conditions of a relatively wide range of laser parameters: power 1.3–1.6 kW, beam diameter 3 mm, traverse speed 250–500 mm/min, powder feed rate 4–12 g/min and overlap coefficient 30–50%.

Interfacial bonding shown in Fig. 6 reveals different thicknesses of planar ZrO_2 crystal from the center to the edge of laser track on AlSi9Cu3 alloy by using the mixed powder with TiO_2 addition. Although some pores occur in the penetration zone of aluminum alloys, good metallurgical continuity exists along the clad/substrate interface. In the area close to the interface between the ZrO_2 layer and aluminum alloy, there formed a thin band of ZrO_2 planar crystals, this being in consistent with the highest temperature gradient at the initial stage of solidification. Several particles of aluminum alloy are also observed near the interface as shown in Fig. 6b by the arrow. From the center to the edge of melt pool as shown in Fig. 6a–d, there exists a tendency to increase thickness of ZrO_2 planar crystal as shown by notations I, II and III. No compositional segregation can be observed in this region of planar crystals. As solidification proceeds, planar growth stops due to interfacial instabilities and local compositional variations, and cellular or columnar solidification occurs within a short distance from the interface. Grain boundaries are featured by the segregation of molten aluminum alloy, which is mixed into the ceramic layer due to excessive laser energy input. Fig. 7 shows the interfacial characterization together with the Al-rich solidified structure in the ceramic layer on AlZn10Si8Mg alloy. From Fig. 7a and b, small amounts of molten aluminum alloy are found to segregate at grain boundary regions located at the bottom of melt pool because of the poor affinity. These aluminum-rich regions in Fig. 7b are considered to be probably due to the penetration of aluminum alloy into the cracked ZrO_2 ceramic layer at the bottom to seal these thermally cracks, which probably forms before the solidification of aluminum alloy. Under optimum cladding conditions, fusion bonding and small dilution by aluminum alloy are produced. It should be noted that the effective bonding observed in this investigation is obtained without the provision of a bond coat, which is commonly used in plasma spraying technique to reduce thermal stress mismatch.

3.3. Phases analysis

The phases formed in the overlapped laser tracks of ZrO_2 ceramic coatings with or without TiO_2 addition

are determined by X-ray diffractometry and compared with those in the initial powder. X-ray diffraction patterns with a step scanning of the initial powder is shown in Fig. 8. It can be seen that the initial YPSZ powder consists of the tetragonal phase (80%), the cubic phase (12%) and the monoclinic phase (8%). No separated yttria peak is detected.

Fig. 9 shows the X-ray diffraction patterns of laser clad ceramic layer without TiO_2 addition on AlSi9Cu3 alloy. The most distinct phase feature of laser clad ZrO_2 ceramic coatings on AlSi9Cu3 alloy is the presence of the non-transformable t' phase and the absence of the monoclinic phase. Rapid solidification during laser cladding hinders the occurrence of c→t thermally activated growth transformation and finally leads to the athermal displacive transformation of cubic to t'. Some workers [11] have also reported the presence of t' in as-sprayed coatings and laser sealed layers.

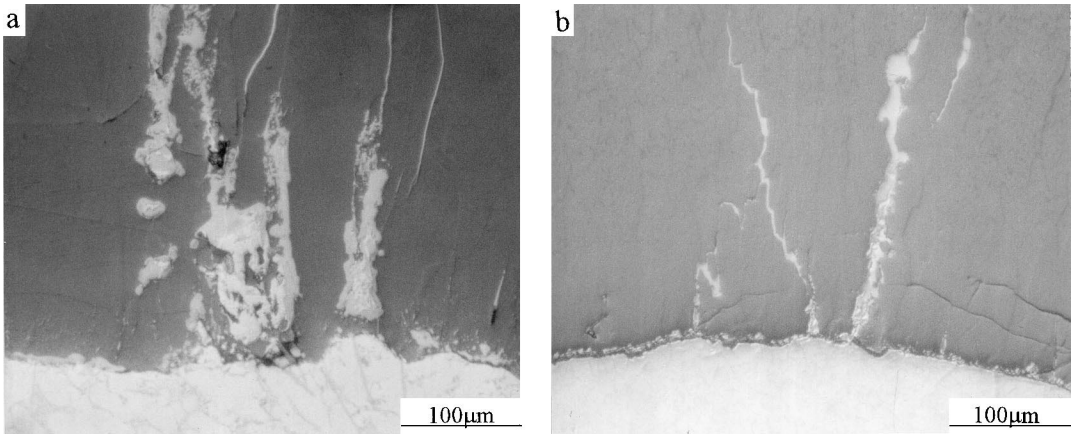

Fig. 7. Interfacial features showing the Al-rich solidified structure in ZrO_2 ceramic layer on AlZn10Si8Mg alloy: (a) isolated or continuous aluminum-rich solidified structure in the ZrO_2 layer near the interface; (b) Al-rich regions around the ZrO_2 grain boundaries near the interface between the cladding and substrate.

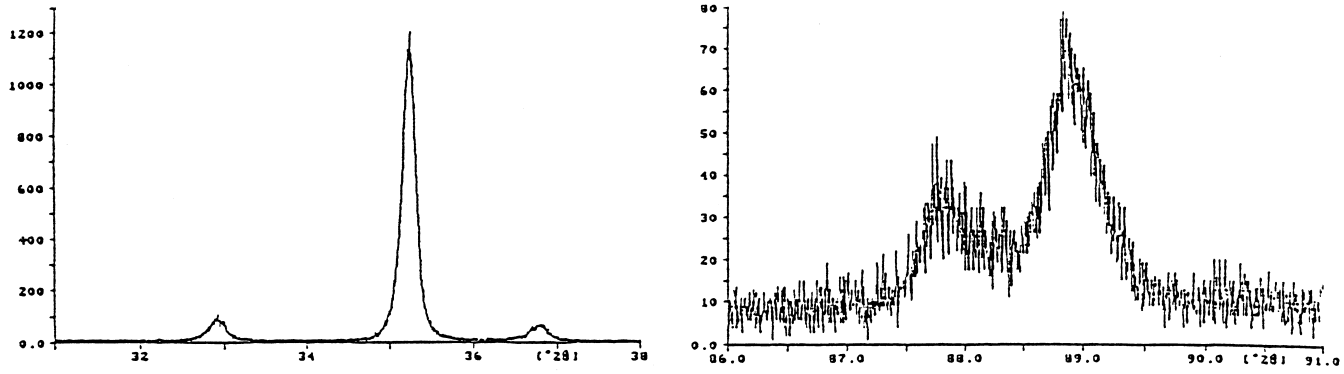

Fig. 8. X-ray diffraction patterns with a step scanning of the initial YPSZ powder.

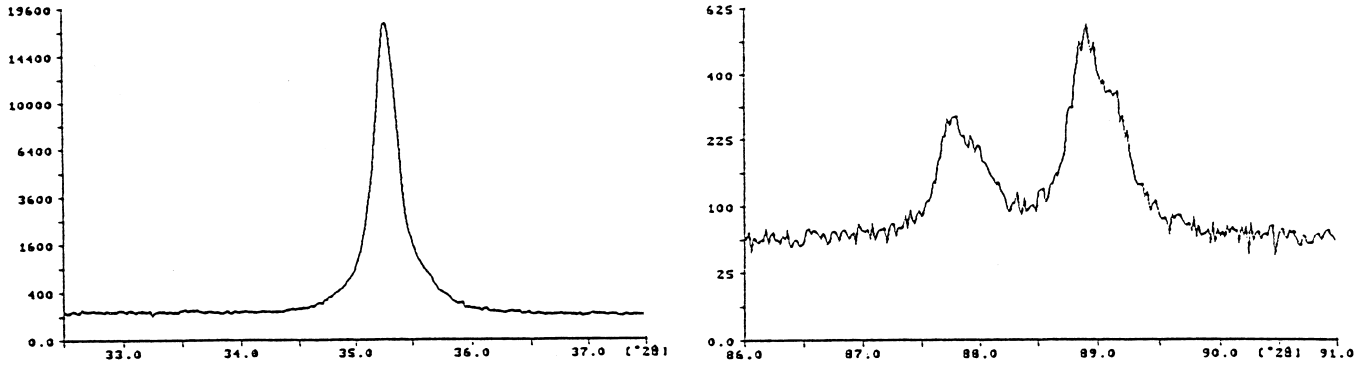

Fig. 9. X-ray diffraction patterns of laser clad ZrO_2 ceramic layer without TiO_2 addition on AlSi9Cu3 alloy.

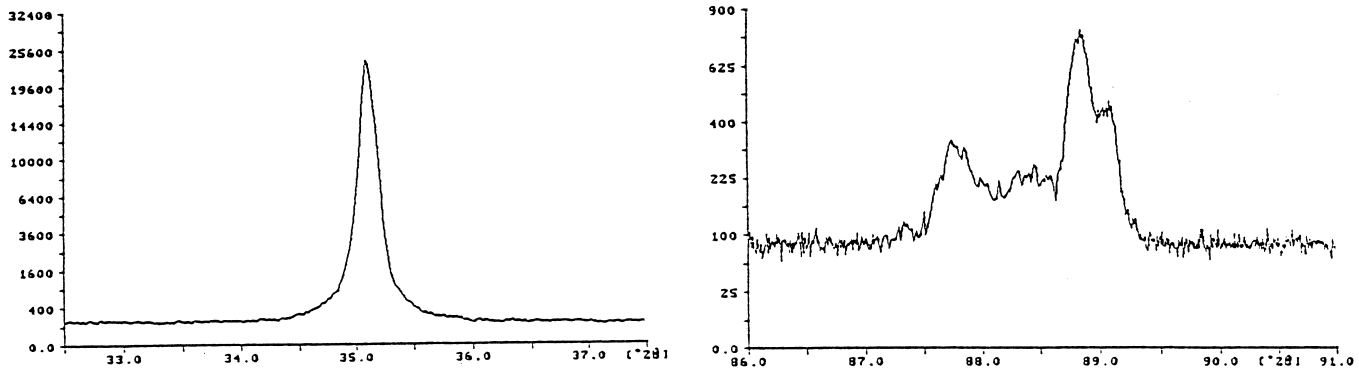

Fig. 10. X-ray diffraction patterns of laser clad ZrO_2 ceramic layer with 2.5 wt.% TiO_2 addition on AlSi9Cu3 alloy.

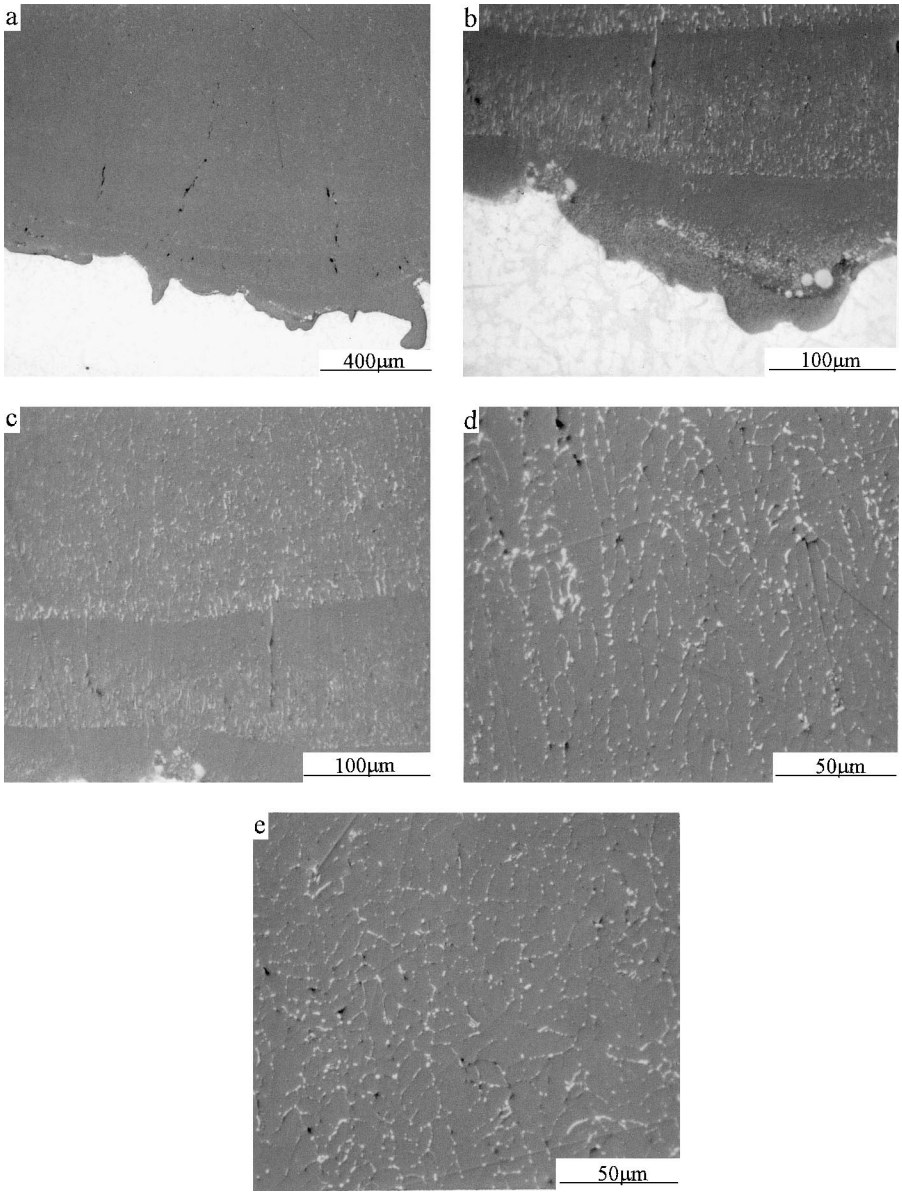

Fig. 11. Microstructural features of ZrO_2 ceramic layers with TiO_2 addition showing the discontinuous segregation of AlSi9Cu3 alloy at the ZrO_2 grain boundaries: (a) low magnification morphology; (b) fine precipitates at the bottom; (c) planar ZrO_2 crystal at the lower region of the melt pool; (d) columnar ZrO_2 structures in the intermediate region; (e) equiaxed structure at the upper region.

Retained cubic phase in the clad ZrO_2 layers was also detected. The t' and c phases were of the same composition, which indicates that the athermal transformation finish temperature is below room temperature. As the coating consisted of t' with retained c-phase, i.e. no metastable t'-phase particles were present, these coatings cannot be toughened by the transformation toughening mechanism. The addition of TiO_2 powders into the ceramic coatings shows no distinct influence on the phase constitution, but a little affect on the contents of various phases present in the ceramic coatings (Fig. 10). From Fig. 10, more retained cubic phase is detected in the ceramic coatings. Three substrates, AlSi10Mg, AlSi9Cu3 and AlZn10Si8Mg alloys, do not exhibit any noticeable differences in the phase constitution of ceramic coatings according to XRD results.

3.4. Microstructural features of ZrO_2 ceramic coatings on aluminum alloys

The microstructure of laser clad ZrO_2 ceramic layer doped with 2.5 wt.% TiO_2 shown in Fig. 11 reveals discontinuous segregation of AlSi9Cu3 alloy at the ZrO_2 grain boundaries. The ceramic layer exhibits distinctly various structures at different thickness regions. At the lower region, two layers of ZrO_2 planar crystals without any compositional segregation have been observed. Fine precipitates of aluminum alloy have also been observed near the interfaces. At the intermediate region, the ceramic layer consists mainly of columnar grains dotted with small amounts of discontinuous segregation of aluminum alloy at the grain boundary regions. At the upper region, equaixed grains of ZrO_2 are formed. The solidified grain boundaries are dotted with many fine precipitates of aluminum alloy. Fig. 12 shows the detailed structure of ZrO_2 ceramic layer on AlZn10Si8Mg alloy. EDX spot analysis demonstrates that the grain boundary regions are rich in aluminum and silicon elements besides the zirconium and oxygen elements. Continuous aluminum-rich grain boundaries are clearly observed on the cross-section of the ceramic layer (Fig. 12a and b). The width of aluminum-rich grain boundary regions varies at different microregions (Fig. 12c). ZrO_2 ceramic grains exhibit a typical columnar

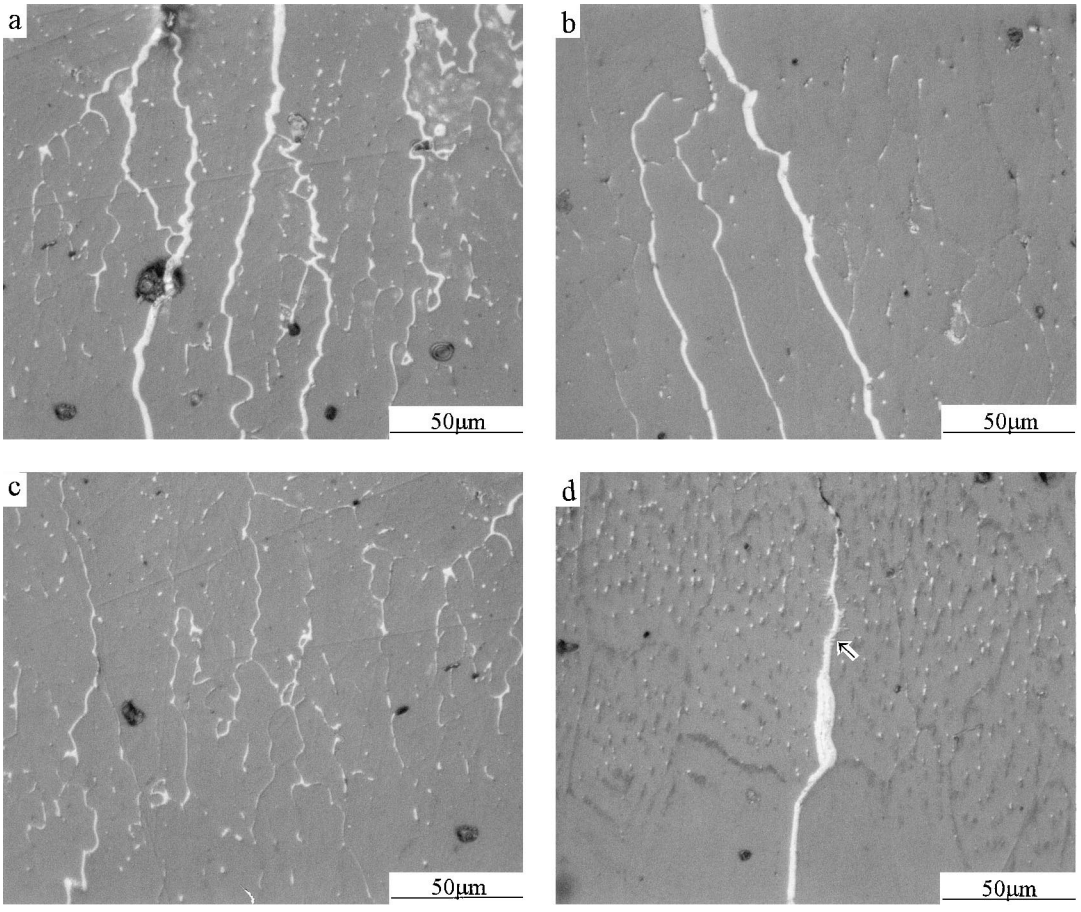

Fig. 12. Microstructural features of ZrO_2 ceramic layers showing the continuous segregation of AlZn10Si8Mg alloy at ZrO_2 grain boundaries within different microregions: (a) widened columnar ZrO_2 grain boundaries caused by continuous segregation of aluminum alloy at the upper region; (b) Al-rich grain boundaries in the intermediate region; (c) narrow grain boundaries in the intermediate region; (d) penetration of aluminum alloy into the cracked ZrO_2 layer at the bottom near the interface.

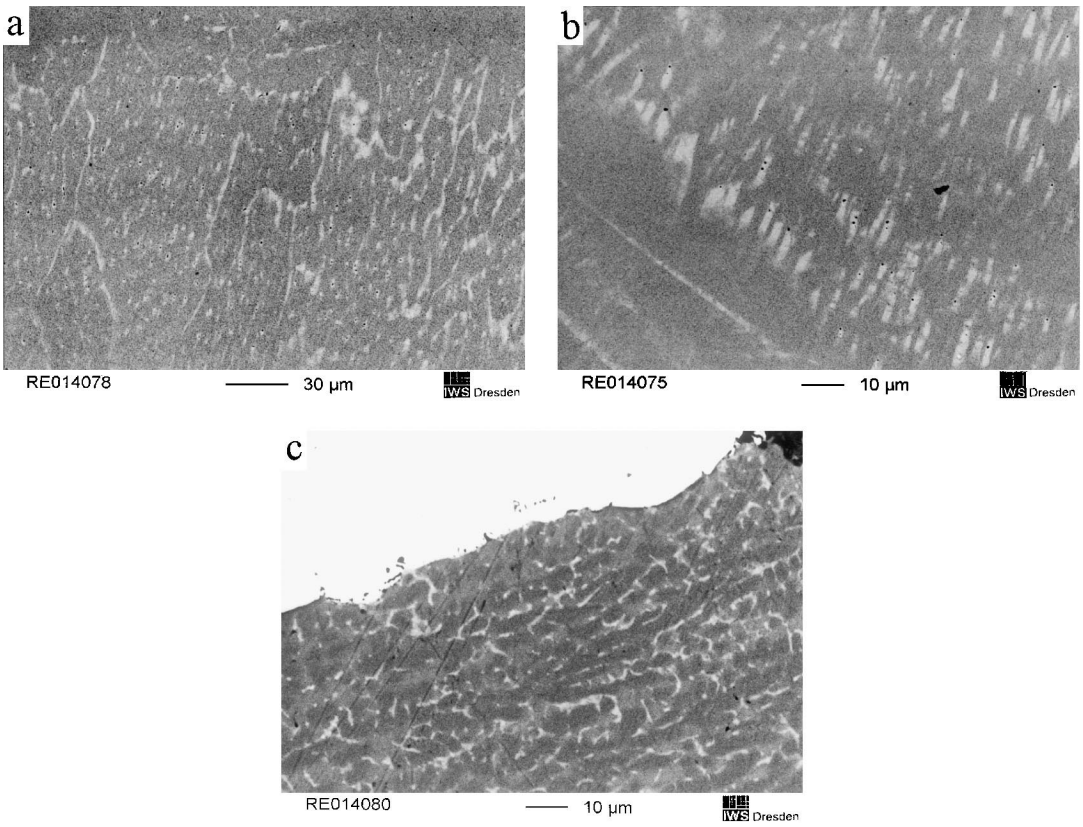

Fig. 13. Microstructural features of ZrO_2 ceramic layer on AlSi10Mg alloy: (a) SEM photographs showing ZrO_2 grains and Al-rich solidified structure at the columnar grain boundaries; (b) and (c) bonding zone featured by planar crystal and the interface morphology.

shape at the intermediate region. A coarse aluminum-rich region is observed at the lower region near the interface as shown in Fig. 12d. Many fine branches of dendritic structure as indicated by the arrow are observed around this primary aluminum-rich structure. This is considered to be probably due to the penetration of aluminum alloy into the cracked ZrO_2 ceramic layer to seal these cracks because of its low melting point. The microstructure of ZrO_2 ceramic layer on AlSi10Mg alloy is also revealed from the cross-sections (Fig. 13). The ceramic layer consists of a resolidified structure featured by columnar grains about 10 μm in width and 100 μm in length. Adjacent to the substrate is a narrow bonding zone (approximately 50 μm) of planar crystals (Fig. 13b). EDX results of the planar bonding zone demonstrate that no distinct compositional changes are detected in the various microregions. The composition in the bonding zone is the same as that within the columnar grains. From Fig. 13c, the interface between the bonding zone and the aluminum alloy is clean and no diffusion layer is detected.

3.5. Microhardness analysis of the ceramic layer

Fig. 14 shows the microhardness curve of laser clad ZrO_2 ceramic layer doped with 2.5 wt.% TiO_2 on AlSi9Cu3 alloy. A distinct hardness step is produced across the interface between the ceramic layer and the penetration zone of aluminum alloy (also see the indents shown in Fig. 4). The hardness of the ZrO_2 ceramic layer is 1415–1575 HV0.1 as shown in Fig. 14, which is substantially larger than that of plasma sprayed coating (600–800 HV0.1). The results of measurement on the overlapped ceramic layer demonstrated no distinct changes in microhardness of the ceramic layer (1267–1590 HV0.1). The enhanced hardness of laser clad ZrO_2 coatings is

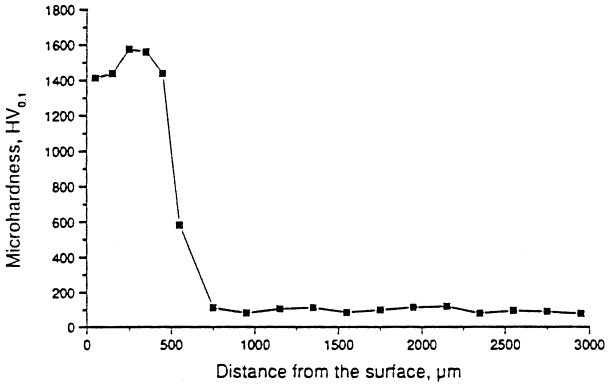

Fig. 14. Microhardness profile of laser-clad ZrO_2 ceramic layer doped with 2.5 wt.% TiO_2 on AlSi9Cu3 alloy.

attributed to the absence of porosity and the relatively fine grain structure of the t' phase as compared with the porous plasma sprayed coatings. The microhardness of the Al-penetration zone with a resolidified structure was found to be 82–114 HV0.1, which is similar to that of the substrate.

4. Conclusions

1. One-step laser cladding technique with a continuous feeding-powder system can be used to produce 7 wt.% yttria partially stabilized zirconia coating with a thickness up to 1.0 mm on different aluminum alloys. For AlZn10Si8Mg alloy, high laser power density and low traverse speed are needed to clad ZrO_2 ceramic coatings with the same thickness in contrast to AlSi10Mg and AlSi9Cu3 alloys. Small amounts of molten AlZn10Si8Mg alloy are observed to flow into the cracked ZrO_2 solidified layer at the bottom to seal these cracks because of its low melting point.
2. The addition of 2.5 wt.% TiO_2 into the YPSZ powder is beneficial to the controllable cracking in the clad layer on AlSi9Cu3 alloy. These claddings on AlSi9Cu3 alloy can be achieved with minimum shrinkage cavities under conditions of a relatively wide range of laser parameters: power 1.3–1.6 kW, beam diameter 3 mm, traverse speed 250–500 mm/min, powder feed rate 4–12 g/min and overlap coefficient 30–50%. The bonding of the claddings to aluminum alloys is satisfactory with small dilution.
3. The ceramic layers on three kinds of aluminum alloys exhibit planar ZrO_2 crystals having different thickness at the lower region, columnar grains in the intermediate region, and equiaxed grains at the upper region. Small amounts of molten aluminum alloys are observed to segregate at the boundary regions of columnar or equiaxed ZrO_2 grains because of the poor affinity. This may be beneficial to reduce the thermal stress concentration during laser cladding.
4. The phases present in the ZrO_2 ceramic layers with or without TiO_2 are mainly non-transformable t' phase together with some amounts of the retained cubic phase. The hardness of the clad ZrO_2 ceramic layer is 1415–1575 HV0.1, which is mainly attibuted to the absence of porosity and fine grains in the ceramic layers.

Acknowledgements

The authors are indebted to Mrs. Wolf, Dr. Techel, Dr. Tangermann, Mrs. Mueller and Mrs. Reinhardt for their help in specimen preparement and SEM observations. J.H. Ouyang is also indebted to the Alexander von Humboldt Foundation for a research fellowship.

References

[1] B.C. Wu, E. Chang, C.H. Chao, M.L. Tsai, J. Mater. Sci. 25 (1990) 1112.
[2] E. Vandehaar, P.A. Molian, M. Baldwin, Surf. Eng. 4 (2) (1988) 159.
[3] K.M. Jasim, R.D. Rawlings, D.R.F. West, J. Mater. Sci. 25 (1990) 4943.
[4] S. Nowotny, A. Richter, K. Tangermann, J. Thermal Spray Technol. 8 (2) (1999) 258.
[5] A. Mueller, A. Techel, S. Nowotny, U. Franz, Laser und Optoelektronik 29 (4) (1997) 48–52.
[6] R. Sivakumar, B.L. Mordike, Surf. Eng. 4 (2) (1988) 127.
[7] A. Petitbon, D. Guignot, U. Fischer, J.M. Guillemot, Mater. Sci. Eng. A121 (1989) 545.
[8] H.L. Tsai, P.C. Tsai, Surf. Coat. Technol. 71 (1995) 53.
[9] D.L. Ruckle, Thin Solid Films 73 (1980) 455–461.
[10] A.S. Grot, J.K. Martyn, Am. Ceram. Soc. Bull. 60 (8) (1981) 807–811.
[11] K.M. Jasim, R.D. Rawlings, D.R.F. West, Mater. Sci. Technol. 8 (1992) 83.